Pharmaceutical Sciences and Drug Design
ISSN: 3062-4428
2023, Volume 3, Page No: 295-311

Available online at: www.galaxypub.co/page/journals

Galaxy Publication

In Silico Evaluation of Anti-Inflammatory Phytochemicals from *Nyctanthes arbor-tristis* Linn Using Molecular Docking and Dynamics Approaches

Grace Y. Tan[1], Wei Ming Lim[2], Hui Xin Ong[3]*, Rachel Koh[1]

[1]Department of Pharmaceutical Sciences, School of Pharmacy, National University of Singapore, Singapore.
[2]Department of Drug Discovery, Faculty of Pharmacy, University of Queensland, Brisbane, Australia.
[3]Department of Medicinal Chemistry, Faculty of Pharmacy, University of Toronto, Toronto, Canada.

***E-mail** ✉ hui.ong@gmail.com

Received: 23 May 2023; **Revised:** 16 August 2023; **Accepted:** 16 August 2023

ABSTRACT

Pharmacological studies on the leaves, flowers, seeds, and bark of Nyctanthes arbor-tristis Linn have confirmed their traditional therapeutic roles in managing diverse health conditions. This research assessed the anti-inflammatory capabilities of 26 plant-derived compounds through molecular docking with AutoDock 4.2, supplemented by Molecular Dynamics Simulations using GROMACS. SwissADME was employed to analyze ADME (absorption, distribution, metabolism, and excretion) profiles. Among these, Arb_E and Beta-sito exhibited robust binding interactions with targets including COX-1, COX-2, PDE4, PDE7, IL-17A, IL-17D, TNF-α, IL-1β, prostaglandin E2, and prostaglandin F synthase. The standard inhibitor celecoxib showed a binding energy of −9.29 kcal/mol, whereas Arb_E stood out with the highest affinity (docking energy: −10.26 kcal/mol). Beta_sito also demonstrated substantial binding with −8.86 kcal/mol against COX-2. In simulations of COX-2 complexed with Arb_E or celecoxib, RMSD values stayed within 0.15 to 0.25 nm, confirming complex stability over the entire duration. Additionally, MM-PBSA calculations indicated that Arb_E's interaction with COX-2 had the most favorable binding energy at −277.602 kJ/mol. Both compounds presented desirable physicochemical properties and drug-likeness in ADME evaluations, suggesting strong therapeutic promise. Hence, these plant constituents may represent viable candidates for anti-inflammatory therapy and require further validation through in vitro and in vivo testing to advance new drug development.

Keywords: Nyctanthes arbor-tristis Linn, Natural products, Anti-inflammatory activity, Cyclooxygenase enzyme inhibition, Binding affinity, Molecular docking simulation

How to Cite This Article: Tan GY, Lim WM, Ong HX, Koh R. In Silico Evaluation of Anti-Inflammatory Phytochemicals from *Nyctanthes arbor-tristis* Linn Using Molecular Docking and Dynamics Approaches. Pharm Sci Drug Des. 2023,3:295-311. https://doi.org/10.51847/ZfL8Qbasl5

Introduction

Nyctanthes arbor-tristis Linn (NAT), an indigenous Indian medicinal species from the Oleaceae family, is additionally grown for ornamental purposes and known locally as night jasmine or harsingar. Its distribution spans sub-Himalayan zones southward to the Godavari region. Reaching up to 10 m in height, the plant features opposite, simple, rough, hairy leaves in decussate arrangement, with flowers clustered at branch tips. It prefers loamy soil with ample moisture and grows well under full sunlight to partial shade. The blooming period usually spans July to October [1, 2].

Various parts of this plant—leaves, flowers, seeds, and bark—have been subjected to pharmacological testing to substantiate traditional uses against ailments like fever, rheumatism, sciatica, arthritis, malaria, and dermatological issues [2, 3].

Key bioactive constituents reported include glycosides, flavonoids, oleanic acid, tannic acid, essential oils, carotene, lupeol, friedeline, benzoic acid, and glucose, each contributing to therapeutic effects. In particular, the anti-inflammatory actions of NAT compounds have drawn increasing research focus lately. Inflammation

involves a multifaceted physiological defense against harmful agents such as pathogens, tissue damage, irritants, and associated toxins, triggering immune activation and secretion of pro-inflammatory factors like prostaglandins, cytokines, and chemokines. Persistent inflammation underlies many pathologies, including rheumatoid arthritis, diabetes, atherosclerosis, and cancer [4].

As a result, discovering safe natural modulators of inflammation that minimize side effects remains a priority. Evidence from animal studies and cellular assays has established NAT's anti-inflammatory efficacy [5, 6]. Notably, leaf extracts display marked bioactivity. These leaves contain flavonoid polyphenols like kaempferol, quercetin, rutin, and astragalin, recognized for antioxidant, anti-inflammatory, and antimicrobial benefits. Triterpenoids identified in the leaves, such as ursolic acid, β-sitosterol, oleanolic acid, and lupeol, are associated with anti-inflammatory, antitumor, and antidiabetic properties [7]. PubChem-registered compounds from this species encompass oleanolic acid, friedelin, 6beta-hydroxyloganin, arborside A, arborside B, 6-beta-hydroxy-loganin, calceolarioside A, astragalin, sitogluside, methyl (1S,4aS)-6-hydroxy-5-[(E)-3-(4-methoxyphenyl)prop-2-enoyl]oxy-7-methyl-1-[(2S,3R,4S,5S,6R)-3,4,5-trihydroxy-6-(hydroxymethyl)oxan-2-yl]oxy-1,4a,5,6,7,7a-hexahydrocyclopenta[c]pyran-4-carboxylate, arbortristoside B, nyctanthic acid, arbortristoside E, arbortristoside D, arbortristoside C, 7-O-(3,4-dihydrocycinnamoyl)nyctanthoside, arborside D, etc.

Certain alkaloids, including nyctanthine and arbortristosides—nitrogenous bases—have shown broad bioactivities encompassing analgesia, spasmolysis, and antimalarial action. Other classes like phenolic acids, lignans, coumarins, fatty acids, and essential oils contribute antioxidant, antibacterial, antifungal, and antiviral effects [8]. The water-soluble fraction obtained from the ethanol extract of NAT leaves has been documented to substantially reduce granuloma formation in cotton pellet assays and edema in carrageenan-challenged rat paws [9]. A methanol extract derived from NAT leaves effectively blocked lipopolysaccharide (LPS)-triggered nitric oxide (NO) release and inducible nitric oxide synthase (iNOS) upregulation in RAW 264.7 macrophage cells, highlighting strong anti-inflammatory capabilities [8]. Additionally, the ethanol extract from NAT leaves diminished secretion of key pro-inflammatory cytokines—including tumor necrosis factor-alpha (TNF-α), interleukin-1 beta (IL-1β), and interleukin-6 (IL-6)—in LPS-activated murine peritoneal macrophages. Several isolated bioactive constituents from NAT leaves have also been pinpointed as prospective Janus kinase (JAK) inhibitors, enzymes central to cytokine signaling pathways that drive rheumatoid arthritis progression [5, 10]. Collectively, these observations point to robust anti-inflammatory attributes in NAT leaves, potentially beneficial for managing inflammation-related diseases. That said, more in-depth investigations are essential to pinpoint precise action mechanisms and establish safety data for the plant and its compounds. The objective of this work was to undertake an in silico evaluation to validate the anti-inflammatory properties of NAT-derived phytochemicals and emphasize the plant's promising role in future anti-inflammatory drug discovery. Certain compounds extracted from NAT leaves and assessed for anti-inflammatory action in LPS-treated RAW 264.7 macrophages include astragalin—a flavonoid glycoside that curbs NO and iNOS activity [11]. The triterpene β-sitosterol notably lowered IL-6, TNF, and IL-1 output in LPS-exposed mouse peritoneal macrophages. Reports indicate that NAT leaves contain high levels of polyphenolic flavonoids, among them kaempferol, quercetin, astragalin, and rutin [4, 12, 13]. Flavonoids in general are recognized for their antioxidant, anti-inflammatory, and antimicrobial benefits [14]. Alkaloids bearing nitrogen atoms demonstrate a range of bioactivities, such as pain relief, spasm reduction, and antimalarial effects. Specifically, arbortristosides A and B have been shown to suppress JAK function while lowering IL-1β, IL-6, and TNF-α concentrations in LPS-challenged macrophages [15]. Lipophilic triterpenoids like beta-sitosterol, ursolic acid, oleanolic acid, and lupeol [12] exhibit anticancer, antidiabetic, and anti-inflammatory actions [14]. How these natural compounds perform against conventional synthetic anti-inflammatory agents can depend on factors like inflammation characteristics, dosage, delivery method, pharmacokinetic profile, and drug interactions. Even so, multiple reports suggest their anti-inflammatory potency matches or exceeds that of standard medications including indomethacin, diclofenac, ibuprofen, and prednisolone [16-19]. Astragalin, for example, matches indomethacin's suppression of NO in LPS-treated RAW 264.7 cells, whereas β-sitosterol outperforms diclofenac in restraining IL-6 in similarly stimulated peritoneal macrophages [18]. Arbortristosides A and B, in turn, inhibit JAKs more effectively than prednisolone in LPS-exposed RAW 264.7 macrophages. Clinical studies in humans are still required, however, to substantiate both efficacy and tolerability for inflammatory conditions [17]. Tackling ongoing inflammation and enhancing patient well-being demand innovative anti-inflammatory therapies. Increasingly, researchers explore botanical sources for safer alternatives with minimal side effects. Here, we aimed to pinpoint natural compounds capable of targeting diverse inflammatory pathways or receptors to boost treatment outcomes and enable lower therapeutic doses. Accordingly, we performed in silico analyses—

encompassing virtual screening, docking, and dynamics simulations—on two NAT phytochemicals: arbortristoside E and beta-sitosterol. Arbortristoside E (PubChem ID:14632884) possesses a molecular weight of 566.5 g/mol and the formula C27H34O13, featuring a sophisticated architecture with esters, hydroxyl groups, and aromatic moieties. Beta-sitosterol (PubChem ID:222284), a phytosterol with a beta-hydroxy substituent, has a molecular weight of 414.7 g/mol and formula C29H50O. Their structural details are illustrated in **Figure 1.**

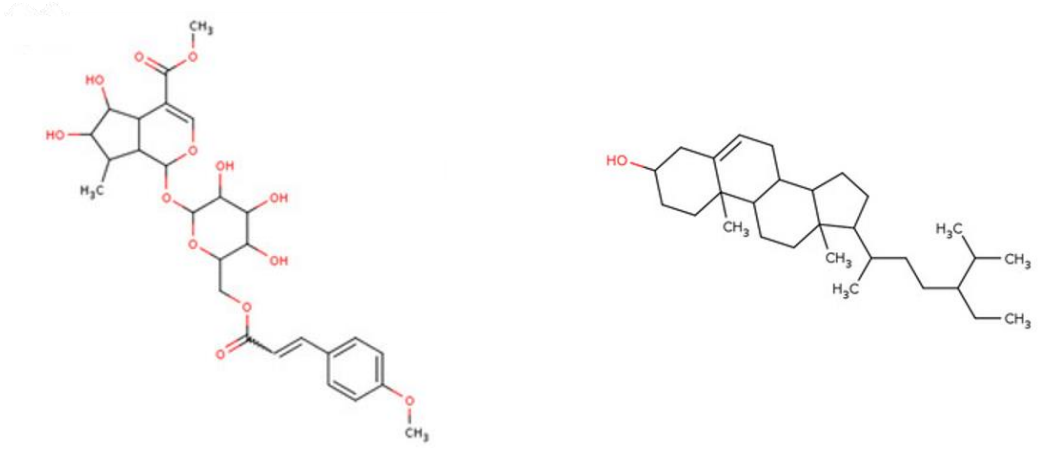

a) b)

Figure 1. Two-dimensional structural representations of (a) arbortristoside E and (b) beta-sitosterol. This marks the inaugural examination of arbortristoside E's therapeutic prospects. On this basis, both arbortristoside E and beta-sitosterol emerge as promising anti-inflammatory candidates, potentially delivering synergistic benefits by targeting distinct receptor sites.

Materials and Methods

Ligand preparation

Selective nonsteroidal anti-inflammatory drugs (NSAIDs) target the COX-2 isoform responsible for elevated prostaglandin production during inflammation. Given their effectiveness in pain relief and management of inflammation-associated diseases, alongside improved gastrointestinal safety compared to non-selective NSAIDs, COX-2-specific inhibitors remain central to anti-inflammatory drug research. Accordingly, we employed the established selective COX-2 inhibitor celecoxib as a benchmark to gauge the anti-inflammatory potential of plant-derived compounds. Following an initial virtual screening of 26 phytochemicals from Nyctanthes arbor-tristis, arbortristoside E (Arb_E) and beta-sitosterol (Beta_sito) emerged as the top candidates based on predicted binding affinities.

Two-dimensional structures and SMILES strings for the primary Nyctanthes arbor-tristis constituents and celecoxib were retrieved from the PubChem database (https://pubchem.ncbi.nlm.nih.gov/) (accessed on 11 October 2023) [20]. These SMILES were subsequently converted to three-dimensional PDB formats using the Novoprolabs server (https://www.novoprolabs.com/tools/smiles2pdb) (accessed on 12 October 2023) [21] in preparation for docking and dynamics studies. Energy minimization of the ligands was then performed in Discovery Studio Visualizer version 21.1.0.20298 [22], applying the CHARMm force field with its empirical energy terms [23, 24].

Receptor preparation

The COX-2 enzyme facilitates prostaglandin biosynthesis, contributing to inflammatory and nociceptive responses. Its human crystal structure (PDB ID: 5F1A) was downloaded from the Protein Data Bank (https://www.rcsb.org/structure/5F1A) (accessed on 19 October 2023) [25].

Water molecules (HOH) and heterogeneous atoms (HETATM) were removed from the original PDB file, followed by energy minimization under the CHARMm force field in Discovery Studio Visualizer version 21.1.0.20298 [23].

Binding site identification was carried out in Discovery Studio Visualizer version 21.1.0.20298 [26], focusing on critical residues to define the active pocket for subsequent docking of the selected phytochemicals.

AutoDock 4.2 tool receptor–ligand docking

In AutoDock 4.2, extraneous elements such as waters and cofactors were stripped from the receptor, followed by addition of polar hydrogens, assignment of charges and atom types, and geometric optimization. For ligands, conformational and tautomeric variants were generated to explore potential binding modes.

A grid box encompassing the active site was configured to map interaction energies, with dimensions of 60 × 60 × 60 points and 0.375 Å spacing. Center coordinates were set as follows: −36.659, −51.728, 2.072 (COX-1), 41.585, 25.501, 237.603 (COX-2), 96.897, 66.877, 19.023 (PDE4), 0.0192, 49.098, 20.118 (PDE7), 79.997, −40.055, −38.557 (IL-17A), 37.218, −35.236, 4.499 (IL-17D), 24.212, 63.416, 44.088 (TNF-α), 11.193, 20.924, −9.834 (IL-1β), and −45.708, −42.479, 0.232 (prostaglandin E2) [27].

Default settings were retained for the docking algorithm, scoring function, and output parameters. Pose generation and orientation relied on the Lamarckian genetic algorithm (LGA) coupled with an empirical free energy function, expressed as:

$$\Delta G_{binding} = \Delta G_{gauss} + \Delta G_{repulsion} + \Delta G_{hbond} + \Delta G_{hydrophobic} + \Delta G_{tors},$$

where ΔG_{gauss} represents attractive Gaussian dispersion, $\Delta G_{repulsion}$ penalizes short contacts, ΔG_{hbond} models directional H-bonding (including metal interactions), $\Delta G_{hydrophobic}$ accounts for non-polar contacts, and ΔG_{tors} scales with rotatable bond count [28].

Upon preparation of receptor, ligand, grid, and parameter files, AutoDock 4.2 was executed with population size (ga_pop_size) of 150, maximum energy evaluations (ga_num_generation) of 2,500,000, 27,000 generations, mutation rate of 0.02, crossover rate of 0.8, and step size of 0.2. Ten independent LGA runs were performed per system, varying with molecular complexity [29].

Docking outcomes were ranked by score, visualized, and benchmarked against controls using Discovery Studio Visualizer version 20.1.0.19295 [26, 30].

Drug-likeness and ADMET

The SwissADME web server (http://www.swissadme.ch) (accessed on 25 October 2023), provided by the Swiss Institute of Bioinformatics (SIB), Lausanne, Switzerland [31-33], was employed to predict the ADME parameters, drug-likeness, and pharmacokinetic profiles of the chosen phytochemicals. Additional toxicity assessments were performed using the pkCSM online platform (http://biosig.unimelb.edu.au/pkcsm/) (accessed on 25 October 2023) [34].

MDS

A 100 ns molecular dynamics simulation (MDS) was carried out on the COX-2–Arb_E, COX-2–Beta_sito, and COX-2–celecoxib complexes with GROMACS version 2018 software [35].

For benchmarking, an additional simulation of apo COX-2 in water was included. The topology for COX-2 was created via the pdb2gmx module, applying the CHARMM27 all-atom force field. Ligand topologies for Arb_E, Beta_sito, and celecoxib were acquired from the SwissParam server [36]. Each system was placed in a triclinic simulation box, solvated with water, and neutralized by adding Na^+ and Cl^- ions. A total of 59 Na^+ and 61 Cl^- ions were introduced to achieve electrical neutrality and a physiological salt concentration of 0.15 M. The fully solvated systems contained 18,793, 18,788, and 18,503 molecules for the COX-2–Beta_sito, COX-2–Arb_E, and COX-2–celecoxib complexes, respectively **(Figures 2a–2c)** [37].

Energy minimization was followed by equilibration in two phases: NVT and NPT ensembles. The steepest descent algorithm was run for 5000 steps. These steps ensured stable temperature and pressure control during the production run [38].

Equilibration was conducted at 300 K and 1.0 bar for 100 ps each. Trajectory analyses utilized gmx rms for root-mean-square deviation (RMSD) [39], gmx rmsf for root-mean-square fluctuation (RMSF), gmx gyrate for radius of gyration (Rg) [40] and gmx hbond for intermolecular hydrogen bond counting. Two-dimensional plots were produced with XMGRACE version 5.1 [41].

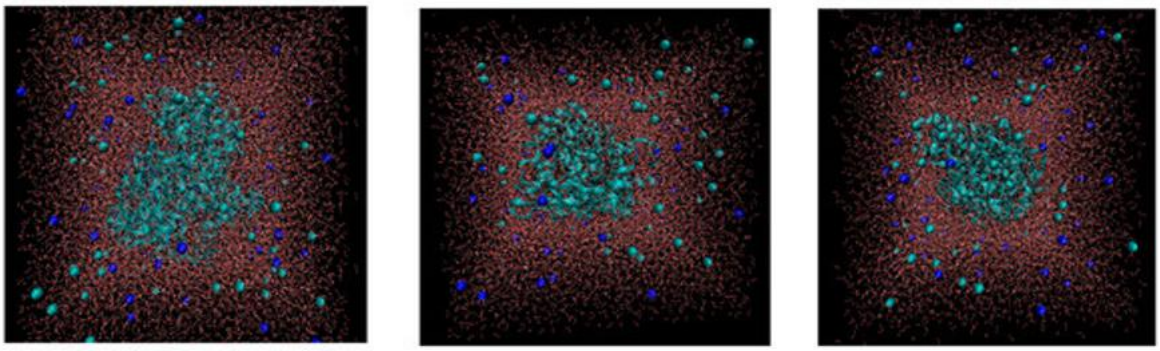

a) b) c)

Figure 2. Three-dimensional representations of the solvated and ionized systems: (a) COX-2–Arb_E, (b) COX-2–Beta_sito, and (c) COX-2–celecoxib. Protein complexes appear as cyan ribbons at the center, surrounded by water with Na^+ (blue spheres) and Cl^- (cyan spheres). Visualizations were generated using VMD (Visual Molecular Dynamics) version 1.9.4a57 [42].

Molecular mechanics-poisson–boltzmann surface area (MM-PBSA)

Following the approach described by Kumari et al. [43, 44], binding free energies for the selected complexes were estimated using the Molecular Mechanics-Poisson–Boltzmann Surface Area (MM-PBSA) method [45]. This technique, implemented through a tool designed for evaluating solvation in biomolecules and macromolecular assemblies, calculates free energy without the entropic term. It comprises two main contributions: the molecular mechanics potential energy in vacuum (ΔGMM), encompassing bonded interactions (bond, angle, dihedral) and non-bonded terms such as van der Waals (ΔGVDW) and electrostatic (ΔGCoulomb) energies, and the solvation free energy (ΔGSolvation), which combines polar (ΔGPolar) and non-polar (ΔGNonpolar) components within an implicit solvent model [42]. The MM-PBSA binding free energy is formulated as follows:

$$\Delta G = \Delta G_{MM} + \Delta G_{solvation} \quad (1)$$

Where

$$\Delta G_{MM} = \Delta G_{Electrostatic\ pot} + \Delta G_{VDW} \quad (2)$$

The solvation energy is the amount of energy necessary to transfer a solute from the void to the solvent and is expressed as the sum of the polar and nonpolar energies (see Equation (3)).

$$\Delta G_{Solvation} = \Delta G_{Polar} + \Delta G_{nonpolar} \quad (3)$$

The polar contribution is closely associated with the formation of permanent dipoles. In contrast, the polar solvation term accounts for permanent dipoles and reflects the solute's charge distribution. For our MM-PBSA computations, the ionic strength was adjusted to 0.150 M through the addition of NaCl. Key setup parameters involved a grid density of 10 points per $Å^2$ and a maximum of 50,000 iterations for the linear Poisson–Boltzmann equation solver.

Results and Discussion

Docking results

In the present investigation, we assessed the prospective anti-inflammatory binding strengths and molecular interactions of the chosen compound Arb_E with various key proteins involved in inflammatory pathways, specifically COX-1, COX-2, PDE4, PDE7, IL-17A, IL-17D, TNF-α, IL-1β, prostaglandin E2, and prostaglandin F synthase. These targets play crucial roles in diverse physiological and pathological events, such as cellular signaling, immune responses, and nociception. Molecular docking was employed to estimate binding energies and inhibition constants (Ki) for Arb_E against each protein, while also examining hydrogen bonding and hydrophobic contacts with active site residues. Key findings are compiled in **Tables 1 and 2**.

Table 1. Docking parameters for Arb_E with the selected targets: COX-1, COX-2, PDE4, PDE7, IL-17A, IL-17D, TNF-α, IL-1β, prostaglandin E2, and prostaglandin F synthase.

Receptors	PDB ID	Binding Energy (kcal/mol)	Inhibition Constant (Ki)	Hydrogen Bond Details	Hydrogen Bond Length (Angstrom)	Residues Involved in Hydrophobic Interaction
Control (Celecoxib)	Cox-2	−9.29	155.52 nM	A:ARG513:HH11—:UNK0:O	2.04571	Val116,Leu359,Tyr335,Ser353,Leu531,His90,Gln192,ALa516,Leu384,Val523,Phe518,Trp387,Met522,Gly526,Leu352,Ala527,Val349,Ser530,Met113
				A:ARG513:CD—:UNK0:O	3.00729	
				A:ARG513:CD—:UNK0:N	3.62419	
COX-1	6Y3C	−3.05	5.81 mM	A:TRP387:HN—:UNK1:O36	1.64895	Ala199,Ala202,Gln203,Thr206,His207,Phe210,Phe381,Asn382,Tyr385,His386,Trp387,His388,Leu390,Met391,Ile444
				UNK1:H49—A:ASN382:O	2.56551	
				UNK1:H50—A:ASN382:OD1	2.53999	
				UNK1:H71—A:TYR385:O	1.92435	
				UNK1:H70—A:TYR385:O	2.23812	
				A:HIS388:CA—:UNK1:O23	3.75406	
				UNK1:C40—A:PHE210:O	3.26066	
COX-2	5F1A	−10.26	30.07 nM	A:ARG120:HE—:UNK1:O38	2.11946	Val116,Arg120,Phe205,Phe209,Gly227,Val228,Tyr348,Val349,Leu352,Ser353,Tyr355,Leu359,Asn375,Ile377,Phe381,Tyr385,Trp387,Phe518,Met522,Val523,Gly526,Ala527,Phe529,Ser530,Leu531,Gly533,Leu534
				A:ASN375:HD22—:UNK1:O32	2.79305	
				A:SER530:HG—:UNK1:O19	2.24954	
				A:SER530:HG—:UNK1:O21	1.89473	
				UNK1:C33—A:GLY533:O	2.89113	
PDE4	2QYK	−9.00	251.54 nM	A:HIS416:HE2—:UNK1:O38	2.03017	Asp413,His416,Ser420,Asn421,Gln422,Leu441,Glu442,His445,Asp484,Met485,Ser486,Asn533,Thr545,Ile548,Phe552,Gln555,Ser567,Met569,Gln581,Phe584
				A:GLN555:HE22—:UNK1:O36	2.64094	
				UNK1:H49—A:ASP484:OD1	1.91855	
				UNK1:H50—A:GLU442:OE2	1.92009	
				A:SER420:CB—:UNK1:O13	3.0371	
				UNK1:C40—A:ASP413:OD1	3.165	
PDE7	1ZKL	−6.74	11.43 uM	A:HIS256:HE2—:UNK1:O34		Tyr211,His212,His216,Asp253,His256,Gly258,Asn260,Gln261,Leu281,Glu282,His285,Ile323,Asp362,Asn365,Trp376,Ser377,Val380,Glu383,Phe384,Gln387,Pro400,Leu401,Cys402,Gln413,Phe416
				A:HIS256:HE2—:UNK1:O35	3.03088	
				A:GLN413:HE22—:UNK1:O32	2.10147	
				UNK1:H69—A:ASP253:OD1	2.53525	
				UNK1:H71—A:GLU282:OE2	2.16071	

				UNK1:H49—A:GLU383:OE2	2.69909	
				UNK1:C40—A:PRO400:O	2.37041	
IL-17A	5HI4	−5.81	54.74 uM	UNK1:H50—A:VAL65:O	1.98348	Leu53,Tyr62,Pro63,Val65,Ile66,Trp67,Gln94,Ile96,Leu97,Val98,Leu99,Val117,Ser118,Val119
				UNK1:H69—A:TYR62:O	2.4814	
				A:PRO63:CD—:UNK1:O35	2.97263	
				A:VAL119:CA—:UNK1:O32	3.01728	
				UNK1:C33—A:TRP67:O	3.37552	
IL-17D	Modeled from MODBASE server	−6.70	12.36 uM	UNK1:H69—A:VAL141:O	2.64013	Ala78,Arg80,Tyr96,Tyr105,Pro106,Tyr108,Leu109,Pro110,Ala112,Thr140,Val141,Val142,Ile163,Pro164,Val165
				UNK1:C40—A:ALA78:O	2.95779	
				UNK1:C33—A:PRO110:O	3.29094	
				UNK1:C33—A:PRO164:O	3.0518	
TNF-α	1A8M	−4.70	360.94 uM	UNK1:C20—A:LEU142:O	3.23102	Pro20,Ala22,Gly24,Lys65,Gly66,Gln67,Asp140,Leu142,Phe144,Ala145
				UNK1:C33—A:GLN67:OE1	3.04695	
IL-1β	6Y8M	−4.59	431.16 uM	A:LYS103:HZ2—:UNK1:O7	2.66882	Lys103,Asn108,Lys109,Leu110,Phe146,Thr147,Met148,Gln149,Phe150
				UNK1:C33—A:PHE150:O	3.21082	
Prostaglandin E2	4YHL	−7.23	4.98 uM	UNK1:H49—A:THR168:OG1	2.63075	Ile23,Pro24,Met27,Val72,Val75,Thr76,Thr79,Tyr80,Leu99,Thr168,Trp169,Cys170,Arg316,Ser319,Val320
				UNK1:H50—A:THR168:O	1.8278	
				UNK1:C40—A:CYS170:O	3.05882	
Prostaglandin F synthase	1RY0	−10.19	33.66 nM	A:TYR24:HN—:UNK1:O7	2.28139	Thr251,Gln279,Asn280,ALA253,Arg276,Leu219,Leu236,Ala269,Leu268,Ala218,Ser221,Gly22,Tyr216,Thr23,Ser51,Lys84,His117
				A:SER217:HN—:UNK1:O36	2.31396	
				A:LYS270:HN—:UNK1:O35	2.95418	
				A:LYS270:HZ2—:UNK1:O23	2.7668	
				A:LYS270:HZ3—:UNK1:O23	2.84067	
				UNK1:H49—A:ASP50:OD2	2.45111	
				UNK1:H49—A:ASP50:O	2.87918	
				UNK1:H50—A:TYR55:OH	2.08453	
				UNK1:C20—A:LYS270:O	2.79899	
				UNK1:C33—A:THR251:OG1	3.62729	

Table 2. Docking parameters for Beta_sito with the selected targets: COX-1, COX-2, PDE4, PDE7, IL-17A, IL-17D, TNF-α, IL-1β, prostaglandin E2, and prostaglandin F synthase.

Receptors	PDB ID	Binding Energy	Inhibition	Hydrogen Bond Details	Hydrogen Bond Length (Angstrom)	Residues Involved in Hydrophobic Interaction
Control (Celecoxib)	Cox-2	−9.29	155.52 nM	A:ARG513:HH11—:UNK0:O	2.04571	Val116,Leu359,Tyr335,Ser353,Leu531,His90,Gln192,ALa516,Leu384,Val523,Phe518,Trp387,Met522,Gly526,Leu352,Ala527,Val349,Ser530,Met113
				A:ARG513:CD—:UNK0:O	3.00729	
				A:ARG513:CD—:UNK0:N	3.62419	
COX-1	6Y3C	−4.91	253.57 uM	NA	NA	Ala199,Phe200,Ala202,Gln203,Thr206,His207,Leu295,Tyr385,His386,Trp387,His388, Leu390,Met391,Tyr404,Leu408,Ile444
COX-2	5F1A	−8.86	320.37 nM	NA	NA	Ala199,Ala202,Gln203,Thr206,His207,Phe210, His214, Asn382,Tyr385,His386,Trp387,His388,Leu390, Leu391
PDE4	2QYK	−8.66	448.17 nM	NA	NA	Tyr371,His372,Asp413,His416,Asn421,Leu441, Glu442, His445,Thr483,Met485,Asp530,Leu531,Ile548,Phe552,Met569,Phe584,Ile588
PDE7	1ZKL	−7.48	3.68 uM	A:HIS256:HE2—:UNK1:O25	2.68409	Tyr211,His212,His216,His252,Asp253,His256,Leu281,Glu282,His285,Thr321,Ile323,Asp362,Val380,Phe384,Leu401,Gln413,Phe416,Leu420
				UNK1:H67—A:ASP253:OD1	2.14352	
IL-17A	5HI4	−7.43	3.60 uM	A:TRP67:HN—:UNK1:O25	2.23528	Tyr62,Pro63,Ile66,Trp67,Ile96,Leu97,Val98,Leu99,Leu112, Val117
				UNK1:H67—A:TRP67:O	1.86307	
IL-17D	Modelled from MODBASE server	−8.22	947.55 nM	UNK1:H67—A:VAL165:O	2.01343	Arg80,Arg81,Phe82,Trp94,Tyr96,Pro106,Tyr108,Pro110,Val165
TNF-α	1A8M	−7.10	6.20 uM	UNK1:H67—A:GLN67:OE1	2.0408	Pro20,Lys65,Gly66,Gln67,Asp140,Tyr141,Leu142,Asp143,Phe144,Ala145
IL-1β	6Y8M	−6.19	29.24 uM	UNK1:H67—A:MET148:O	2.23593	Leu6,Met44,Phe46,Lys103,Glu105,Asn108,Leu110,Thr147,Met148,Gln149,Phe150

Prostaglandin E2	4YHL	−8.58	514.41 nM	NA	NA	Ile23,Pro24,Met27,Thr69,Val72,Ser73,Thr76,Tyr80,Arg316,Ser319,Val320
Prostaglandin F synthase	1RY0	−7.39	3.83 uM	NA	NA	Arg223,Leu236,Gly220,Leu219,Ala218,Ala269,Tyr55,Ser217,Tyr55,Tyr24,Tyr216,Gly22,Asp50,Leu268,Thr23,Lys270,Gln222,Ser221

The reference compound celecoxib, a selective NSAID, exhibited strong affinity for cyclooxygenase-2 (COX-2), recording a binding energy of −9.29 kcal/mol, reflecting robust interaction. Its inhibition constant (Ki) was 155.52 nM, indicating effective COX-2 suppression at nanomolar concentrations or below.

Table 1 further details hydrogen bonding between celecoxib and COX-2: one bond links the carboxylate of ARG513 (COX-2) to the hydroxyl of UNK0 (celecoxib) at 2.04571 Å, another connects the same ARG513 carboxylate to the amide of UNK0 at 3.00729 Å, and a third involves the ARG513 carboxylate with the amine of UNK0 at 3.62419 Å **(Table 1)**.

Additionally, extensive hydrophobic contacts contributed to stability, involving COX-2 residues Val116, Leu359, Tyr335, Ser353, Leu531, His90, Gln192, Ala516, Leu384, Val523, Phe518, Trp387, Met522, Gly526, Leu352, Ala527, Val349, Ser530, and Met113 **(Figures 3a and 3b).** Such non-polar interactions enhance complex stabilization by aligning hydrophobic regions of ligand and protein.

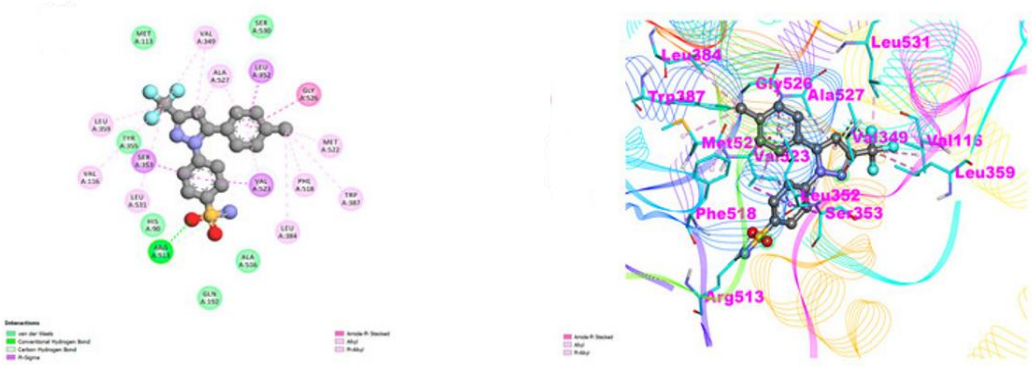

a) b)

Figure 3. (a) Two-dimensional interaction diagram and (b) three-dimensional view of celecoxib bound to COX-2.

Compounds targeting COX-1 and COX-2 remain primary choices for developing anti-inflammatory and pain-relieving medications [46].

Arb_E displayed weak interaction with COX-1, yielding a binding energy of −3.05 kcal/mol and a Ki of 5.81 mM. Binding involved hydrogen bonds with Tyr385 and Asn382, plus hydrophobic contacts with Phe210 and Pro400 **(Table 1).** In contrast, Arb_E demonstrated markedly stronger affinity for COX-2 (−10.26 kcal/mol, Ki: 30.07 nM), mediated by three hydrogen bonds to Arg120, Asn375, and Ser530, along with four hydrophobic interactions involving Gly533, Trp67, Pro110, and Pro164 **(Figures 4a and 4b, Table 1).**

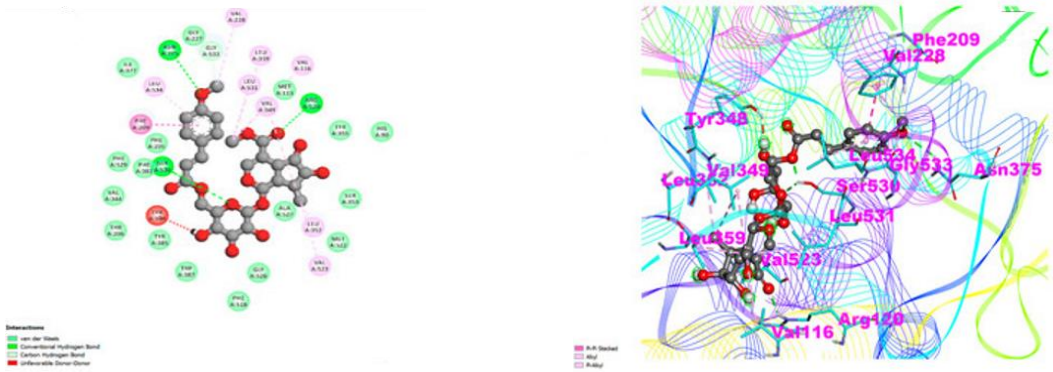

a) b)

Figure 4. (a) Two-dimensional interaction diagram and (b) three-dimensional view of Arb_E bound to COX-2.

The docking outcomes reveal that Arb_E preferentially inhibits COX-2 over COX-1, a favorable profile that may minimize adverse effects linked to COX-1 blockade, including gastric irritation and ulceration. Notably, Arb_E also showed strong binding to both COX-2 and prostaglandin E2 (PGE2), a downstream inflammatory mediator produced by COX-2. This dual targeting implies potential synergistic anti-inflammatory effects through reduced PGE2 synthesis.

PDE4 and PDE7 catalyze the hydrolysis of cyclic adenosine monophosphate (cAMP), an important second messenger regulating numerous cellular functions. Agents inhibiting PDE4 and PDE7 have emerged as promising candidates for treating inflammatory disorders, including asthma, chronic obstructive pulmonary disease (COPD), psoriasis, and rheumatoid arthritis [47].

Both compounds investigated here demonstrated strong binding to PDE4, exhibiting a binding energy of −9.00 kcal/mol and a Ki of 251.54 nM. Hydrogen bonding occurred with the PDE4 residues His416, Glu442, Asp484, and Gln555, while four hydrophobic interactions involved Ser420, Asp413, Pro400, and Leu401. In contrast, a moderate yet noteworthy affinity for PDE7 was recorded, with a binding energy of −6.74 kcal/mol and a Ki of 11.43 μM. Four hydrogen bonds were detected with PDE7 residues Asp253, Glu282, Glu383, and Gln413. Numerous reports have established that natural plant-derived bioactives can suppress PDE activity to manage diverse inflammatory disorders **(Table 1).** Several promising plant-based PDE inhibitors have been identified, including coumarins (glycocoumarin and licoarylcoumarin), agapanthus saponins (saponin, lignin, kobusin, and (±)-schizandrin), terpenes (perianradulcin A, ursolic acid, and quinovic acid), anthraquinones (chrysophanol and emodin), and alkaloids (Sanjoinine-D) [48].

IL-17A and IL-17D belong to the IL-17 cytokine family and play key roles in inflammatory processes, immune regulation, and cellular signaling. IL-17A serves as the primary cytokine produced by Th17 cells, contributing to host protection against pathogens as well as to autoimmune pathologies. IL-17D, though less characterized, is produced by multiple tissues and cell types and has been linked to tumor suppression and antiviral responses [49]. Docking analyses revealed meaningful interactions of the compounds with both IL-17A and IL-17D (binding energies of −5.81 and −6.70 kcal/mol, with Ki values of 54.74 and 12.36 μM, respectively). For IL-17A, two hydrogen bonds involved Val65 and Tyr62, accompanied by four hydrophobic contacts with Leu53, Pro63, Trp67, and Gln94. For IL-17D, four hydrogen bonds engaged Val141, Glu282, Glu383, and Gln413, with four hydrophobic interactions involving Ala78, Pro110, Pro164, and Cys402 **(Table 1).** The documented anti-inflammatory effects of various phytochemicals acting via IL-17A and IL-17D pathways underscore the relevance of these observations. These results indicate that the examined natural compound can engage both IL-17A and IL-17D, potentially modulating inflammatory signaling cascades. Further experimental validation is required to elucidate its biological impact on these cytokines.

Tumor necrosis factor-alpha (TNF-α) and interleukin-1 beta (IL-1β) are major pro-inflammatory cytokines orchestrating numerous immune and inflammatory reactions [19]. They contribute to pathologies such as rheumatoid arthritis, ulcerative colitis, Alzheimer's disease, and Crohn's disease. Targeted inhibitors of TNF-α and IL-1β have been successfully developed as therapeutics for these conditions [50].

The compounds displayed notable binding to TNF-α (−4.70 kcal/mol, Ki: 360.94 μM). Specifically for IL-1β, interaction yielded a binding energy of −4.59 kcal/mol and Ki of 431.16 μM, without hydrogen bond formation. Only one hydrogen bond was observed with Lys103 of IL-1β, alongside one hydrophobic contact with Phe150. Overall, these findings suggest moderate inhibitory potential against TNF-α and IL-1β. Binding affinities of the compounds to TNF-α and IL-1β were weaker than those of their endogenous ligands to TNFR1 and IL-1 receptor 1, respectively, implying minimal disruption of physiological cytokine signaling.

Prostaglandin F synthase (PGFS), an enzyme in the aldo-keto reductase (AKR) superfamily, converts prostaglandin D2 (PGD2) to prostaglandin F2α (PGF2α). Interaction showed a binding energy of −10.19 kcal/mol and Ki of 33.66 nM. Ten hydrogen bonds were formed, and hydrophobic interactions involved residues Thr251, Gln279, Asn280, ALA253, Arg276, Leu219, Leu236, Ala269, Leu268, Ala218, Ser221, Gly22, Tyr216, Thr23, Ser51, Lys84, and His117 **(Table 1).**

In addition, we examined the binding profiles of beta-sitosterol—a phytosterol known for cholesterol reduction and anti-inflammatory activity—against the same panel of targets: COX-1, COX-2, PDE4, PDE7, IL-17A, IL-17D, TNF-α, IL-1β, prostaglandin E2, and prostaglandin F synthase. These proteins participate in inflammation, pain sensation, immune modulation, and cellular signaling. Outcomes are presented in **Table 2**.

COX-1 and COX-2 enzymes convert arachidonic acid into prostaglandins, mediators of inflammation, pain, fever, and other processes. Cyclooxygenase inhibitors remain cornerstone treatments for inflammation and analgesia.

Beta-sitosterol exhibited moderate affinity for COX-1 (−4.91 kcal/mol, Ki: 253.57 µM), relying solely on multiple hydrophobic contacts without hydrogen bonds, thereby maintaining complex stability.

Stronger binding was seen with COX-2 (−8.86 kcal/mol, Ki: 320.37 nM) **(Table 2).** Again, no hydrogen bonds formed, but 18 hydrophobic interactions with various COX-2 residues were noted. The docking configuration for beta-sitosterol in COX-2 is illustrated in **Figures 5a and 5b**. These data position beta-sitosterol as a preferential COX-2 inhibitor, a property that could limit COX-1-related adverse effects like gastrointestinal bleeding and ulceration [51, 52]. Furthermore, beta-sitosterol outperformed prostaglandin E2 (PGE2), the endogenous COX-2 substrate, in binding affinity [53], suggesting competitive inhibition and reduced prostaglandin synthesis.

PDE4 and PDE7 hydrolyze cyclic adenosine monophosphate (cAMP), a critical second messenger. Their inhibitors hold therapeutic promise for conditions including rheumatoid arthritis, COPD, asthma, and psoriasis [54]. Beta-sitosterol bound robustly to PDE4 (−8.66 kcal/mol, Ki: 448.17 nM) **(Table 2),** stabilized by 17 hydrophobic contacts without hydrogen bonds. Affinity for PDE7 was also substantial (−7.48 kcal/mol, Ki: 3.68 µM), featuring two hydrogen bonds with His256 and Asp253 [55, 56] **(Table 2).**

IL-17A and IL-17D, part of the IL-17 cytokine family, regulate inflammation, immunity, and signaling. IL-17A, the hallmark cytokine of Th17 cells, influences pathogen defense and autoimmunity [57].

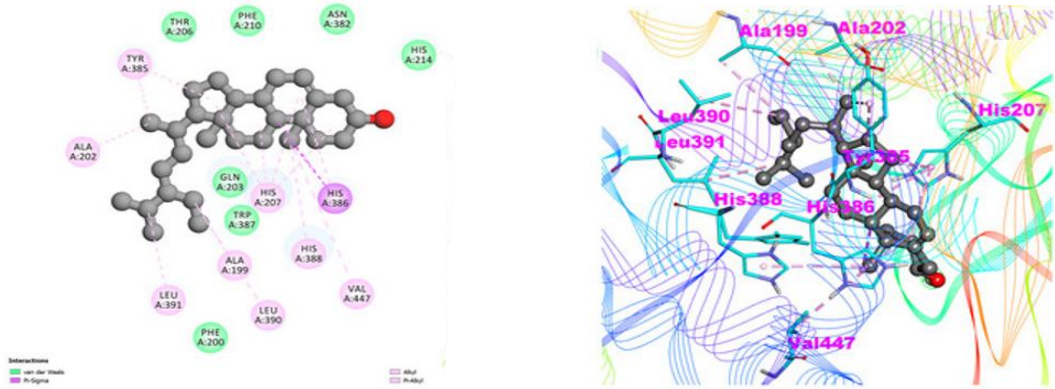

a) b)

Figure 5. (a) Two-dimensional interaction map and (b) three-dimensional visualization of Beta_sito docked with COX-2.

The cytokine IL-17D, which receives comparatively less research attention, is produced by numerous cell types and tissues and has roles in suppressing tumors and combating viral pathogens. Beta_sito displayed robust affinity toward IL-17A (−7.43 kcal/mol binding energy, Ki: 3.60 µM) **(Table 2),** establishing one hydrogen bond with Trp67 and 11 hydrophobic interactions across various residues. Likewise, it bound strongly to IL-17D (−8.22 kcal/mol, Ki: 947.55 nM) **(Table 2),** forming a hydrogen bond with Val165 alongside nine hydrophobic contacts involving multiple residues **(Table 2).** Such outcomes point to Beta_sito's ability to target both IL-17A and IL-17D, possibly altering their associated signaling cascades. That said, the precise functional impacts of Beta_sito on these cytokines remain undetermined and require additional studies.

TNF-α and IL-1β represent key pro-inflammatory cytokines driving diverse immune and inflammatory pathways. These mediators are implicated in disorders including rheumatoid arthritis, Crohn's disease, ulcerative colitis, and Alzheimer's disease. Specific blockers of TNF-α and IL-1β have been engineered into effective anti-inflammatory therapies. Beta_sito revealed strong interaction with TNF-α (−7.10 kcal/mol, Ki: 6.20 µM), supported by a single hydrogen bond to Gln67 and ten hydrophobic engagements with assorted residues. Its binding to IL-1β was less pronounced but still relevant (−6.19 kcal/mol, Ki: 29.24 µM) **(Table 2),** featuring one hydrogen bond with Met148 and nine hydrophobic links to other residues. Taken together, this positions Beta_sito as an effective TNF-α blocker with moderate activity against IL-1β, potentially dampening their contributions to inflammation. Intriguingly, Beta_sito outperformed the native receptors TNFR1 and IL-1R1 in binding strength to TNF-α and IL-1β, respectively, raising the possibility of disrupting endogenous cytokine pathways [58-60].

Docking with prostaglandin F synthase (PGFS) produced a binding energy of −7.39 kcal/mol and Ki of 3.83 µM. Hydrogen bonding was absent, but complex stability relied on hydrophobic contributions from residues Arg223,

Leu236, Gly220, Leu219, Ala218, Ala269, Tyr55, Ser217, Tyr55, Tyr24, Tyr216, Gly22, Asp50, Leu268, Thr23, Lys270, Gln222, and Ser221 **(Table 2).**

ADMET results

ADME encompasses the core processes of absorption, distribution, metabolism, and excretion that shape a molecule's fate within the organism. Celecoxib is forecasted to possess high gastrointestinal absorption and capability to traverse the blood–brain barrier (BBB). It is also flagged as a P-glycoprotein (Pgp) substrate—an active efflux mechanism—and as an inhibitor of key metabolizing enzymes CYP1A2, CYP2C19, and CYP2C9. Its skin permeability metric (log Kp) stands at −6.21, reflecting limited transdermal potential. In comparison, Arb_E is projected to show poor gastrointestinal uptake and no BBB penetration, without Pgp substrate properties or CYP inhibition. Its markedly low log Kp of −9.95 highlights negligible skin permeation. Beta_sito mirrors low gastrointestinal absorption and lacks BBB permeability, Pgp involvement, or CYP inhibitory effects, yet its log Kp of −2.2 denotes reasonably better skin penetration. These insights aid in tailoring compounds toward specific therapeutic needs—for instance, steering clear of Pgp substrates or CYP inhibitors when central nervous system activity is targeted, or selecting candidates with higher (less negative) log Kp for topical applications.

As a clinically approved agent for managing pain and inflammation, celecoxib has a molecular weight of 381.37 g/mol, four rotatable bonds, seven acceptors and one donor for hydrogen bonding, and a TPSA of 86.36 Å². Its consensus log P of 3.4 aligns well with optimal ranges for drug candidates. Compliance with all major filters—Lipinski, Ghose, Veber, Egan, and Muegge—predicts favorable oral bioavailability and stability. The compound earns a bioavailability score of 0.55 (satisfactory) and a synthetic accessibility rating of 2.74, implying straightforward chemical synthesis.

To our knowledge, Arb_E remains untested in clinical settings. It possesses a molecular weight of 566.55 g/mol, 10 rotatable bonds, 5 hydrogen bond acceptors, and 13 hydrogen bond donors. Its topological polar surface area measures 190.67 Å², with a consensus log P of −0.14. The compound breaches Lipinski's rule regarding hydrogen bond acceptors but complies with the remaining criteria. Consequently, it is likely to exhibit limited oral bioavailability and metabolic stability, consistent with its low bioavailability score of 0.11. Its synthetic accessibility score stands at 6.51, indicating considerable synthetic complexity.

Beta-sitosterol, a plant-derived sterol, is recognized for its notable antioxidant and anti-inflammatory activities. It has a molecular weight of 414.71 g/mol, six rotatable bonds, one hydrogen bond acceptor, and one hydrogen bond donor. Its polar surface area is 20.23 Å², and the consensus log P is 7.19. It infringes Lipinski's rule on molecular weight while adhering to the others, pointing to potential challenges in oral bioavailability and metabolic stability. The bioavailability score is 0.55, considered modest, and its synthetic accessibility is 6.3, reflecting relative difficulty in synthesis.

Its molecular weight, rotatable bonds, TPSA, and consensus log P all fall within optimal ranges, with full adherence to the Lipinski, Ghose, Veber, Egan, and Muegge filters. It also benefits from a favorable bioavailability score and easier synthesis. Although Arb_E and beta-sitosterol display certain drug-like features, they may serve as starting points for developing new anti-inflammatory agents.

As an established therapeutic for pain and inflammation, celecoxib is forecasted to exhibit mutagenicity, albeit below the toxicity threshold. Its maximum tolerated dose (MTD) is 0.021 log(mg/kg/day), also below the threshold. It shows no predicted inhibition of hERG I or hERG II channels, which regulate cardiac repolarization. The oral rat acute toxicity (LD50) is 2.027, exceeding the toxicity cutoff, while the chronic toxicity (LOAEL) is 0.963, falling below it. No hepatotoxicity or skin sensitization is anticipated, nor toxicity toward T. pyriformis or fathead minnows.

Arb_E, an unexplored candidate in humans, is not forecasted to be mutagenic. Its MTD is −0.151 log(mg/kg/day), below the threshold. No hERG I or II inhibition is predicted. The LD50 in oral rat studies is 3.197 (above threshold), and LOAEL is 3.25 (above threshold). Hepatotoxicity, skin sensitization, and toxicity to T. pyriformis or minnows are not expected.

Beta-sitosterol, known for anti-inflammatory and antioxidant effects, is similarly non-mutagenic in predictions. Its MTD is −0.621 log(mg/kg/day), below the threshold. No hERG inhibition is foreseen. Oral rat LD50 is 2.552 (above threshold), while LOAEL is 0.855 (below threshold). It is not projected to cause hepatotoxicity, skin sensitization, or harm to T. pyriformis or minnows.

Overall, celecoxib emerges as the least concerning in terms of predicted toxicity, remaining below thresholds across categories. Arb_E and beta-sitosterol raise minor flags but largely stay below thresholds in most areas.

Importantly, these are computational estimates only, real-world performance may vary, underscoring the need for empirical validation through experimental testing.

Molecular dynamics and simulation analysis

Following completion of the simulations, trajectory data from GROMACS 2018 were processed using XMGRACE version 5.1. Two-dimensional plots were generated to evaluate root-mean-square fluctuation (RMSF), root-mean-square deviation (RMSD), radius of gyration (RoG), and hydrogen bonding over a 100 ns timeframe.

The Beta_sito–COX-2 complex exhibited the highest RMSD, reaching 0.3 nm, while maintaining stable trajectories. In contrast, apo COX-2 (in water), COX-2–Arb_E, and COX-2–celecoxib complexes displayed deviations between 0.15 and 0.25 nm **(Figure 6a).** The COX-2 and COX-2–Arb_E systems averaged around 0.2 nm. RMSF values across complexes spanned 0.1 to 0.9 nm, with most averaging near 0.1 nm except for notable peaks in the 70–100 residue segment **(Figure 6b).**

Radius of gyration metrics reflect structural compactness and folding stability, providing insight into protein integrity when bound to ligands. Values ranged from 2.43 to 2.52 nm across systems. Apo COX-2, Beta_sito-bound, and celecoxib-bound complexes clustered near 2.46 nm. The Arb_E complex registered slightly elevated values above 2.46 nm, with a generally steady profile aside from minor variations between 20 and 40 ns **(Figure 6c).**

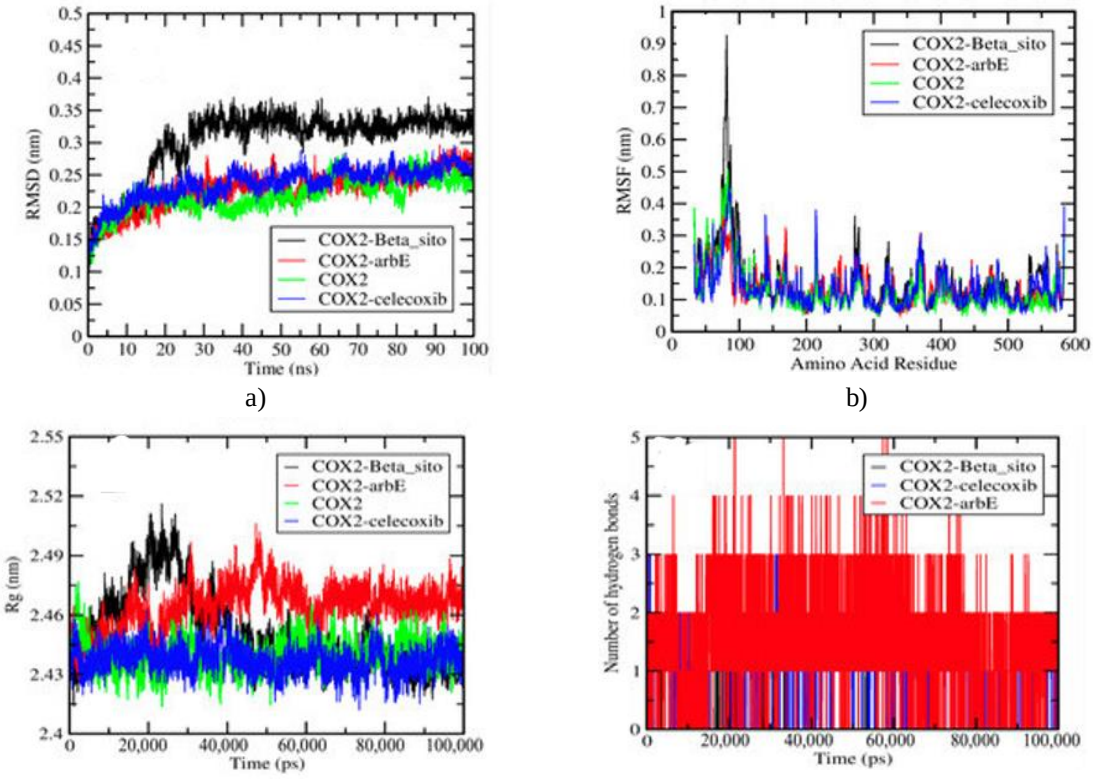

Figure 6. Trajectory-derived plots. (a) RMSD trajectories for the COX-2–Beta_sito complex (black), COX-2–Arb_E complex (red), apo COX-2 in water (green), and COX-2–celecoxib complex (blue). (b) RMSF profile illustrating per-residue fluctuations. (c) Radius of gyration (Rg) graph depicting the structural compactness and folding of COX-2 when bound to Beta_sito, Arb_E, or celecoxib. (d) Graph displaying the count of intermolecular hydrogen bonds across the 100 ns simulation for the selected complexes.

Hydrogen bonding is critical for stabilizing ligand–protein complexes and serves as a key metric in evaluating interaction strength and thermodynamic properties [61]. The hydrogen bond analysis revealed that the COX-2–Arb_E complex maintained five hydrogen bonds throughout the simulation, whereas the COX-2–Beta_sito complex sustained only one. The COX-2–celecoxib complex, in comparison, formed three hydrogen bonds **(Figure 6d).**

MM-PBSA results

We conducted a comparative binding free energy assessment for the ligands Arb_E, Beta_sito, and celecoxib within their respective COX-2 complexes (COX-2–Arb_E, COX-2–Beta_sito, and COX-2–celecoxib), with results compiled in **Table 3**. The calculated binding free energies (ΔGbind) showed that Arb_E achieved the most favorable value of −277.602 kJ/mol, surpassing Beta_sito (−214.385 kJ/mol) and celecoxib (−193.635 kJ/mol). Net differences highlighted substantial advantages: −83.967 kJ/mol (Arb_E versus celecoxib), −63.217 kJ/mol (Arb_E versus Beta_sito), and −20.75 kJ/mol (Beta_sito versus celecoxib), underscoring stronger binding energetics for Arb_E and Beta_sito relative to the reference compound.

Table 3. Components of binding free energy for the selected complexes derived from MM-PBSA calculations.

S.N0.	Ligands	Van der Wall Energy (kJ/mol)	Electrostatic Energy (kJ/mol)	Polar Salvation Energy (kJ/mol)	SASA Energy (kJ/mol)	Binding Energy (kJ/mol)
1.	Arb_E	−300.730 +/−13.113	−22.633 +/−9.119	47.260 +/−188.830	−28.499 +/−0.977	−277.602 +/−39.964
2.	Beta_sito	−232.379 +/−11.525	−0.160 +/−2.069	39.170 +/−34.210	−21.016 +/−1.008	−214.385 +/−36.906
3.	Celecoxib	−220.267 +/−0.184	−59.621 +/−0.124	103.2250 +/−0.94	−16.972 +/−0.011	−193.635 +/−0.573

Through molecular docking, we examined the binding profiles of Beta_sito—a phytosterol recognized for its anti-inflammatory effects—against multiple targets: COX-1, COX-2, PDE4, PDE7, IL-17A, IL-17D, TNF-α, IL-1β, prostaglandin E2, and prostaglandin F synthase. The results position Beta_sito as a preferential COX-2 inhibitor over COX-1, a dual inhibitor of PDE4 and PDE7, a strong inhibitor of TNF-α, and a moderate inhibitor of IL-1β. High affinities were also observed for IL-17A and IL-17D, although the physiological consequences on these cytokines remain to be clarified. Overall, Beta_sito holds promise as a therapeutic candidate for inflammatory conditions, pending further validation of its in vivo effects.

Conclusion

In silico methodologies have greatly advanced drug discovery and development, especially within the field of anti-inflammatory research. The intricate architecture of biological systems poses difficulties in accurately modeling and predicting drug impacts. Additionally, limited experimental validation data and potential unsuitability of certain compounds or targets for computational analysis present further challenges. Despite these limitations, computational strategies have successfully identified promising hit compounds, advancing them through the drug development pipeline and occasionally to market approval. Ongoing efforts focus on enhancing model accuracy and dependability by integrating more empirical evidence and refining algorithmic approaches.
Molecular docking was applied to evaluate the binding affinities and interaction patterns of the novel compound with multiple targets: COX-1, COX-2, PDE4, PDE7, IL-17A, IL-17D, TNF-α, IL-1β, prostaglandin E2, and prostaglandin F synthase. The compound demonstrated selectivity for COX-2 inhibition over COX-1, dual inhibition of PDE4 and PDE7, and moderate binding to IL-17A and IL-17D. Conversely, weaker affinities were observed toward TNF-α and IL-1β, suggesting minimal influence on their pro-inflammatory pathways. Overall, the compound exhibits promise as a therapeutic agent for inflammatory disorders. Subsequent investigations are essential to corroborate these computational outcomes experimentally. Thus, the examined natural compounds emerge as prospective anti-inflammatory candidates, warranting additional in vitro and in vivo testing to facilitate the creation of new anti-inflammatory therapeutics. The provided insights may guide the pharmaceutical sector in pursuing novel anti-inflammatory drug development.

Acknowledgments: None

Conflict of Interest: None

Financial Support: None

Ethics Statement: None

References

1. Sana T, Khan M, Siddiqui BS, Baig TA, Jabeen A, Begum S, et al. Anti-inflammatory and urease inhibitory iridoid glycosides from Nyctanthes arbor-tristis Linn. J Ethnopharmacol. 2024;319:117368.
2. Chakraborty R, De SD. A brief overview on the health benefits of Nyctanthes arbor-tristis Linn.—a wonder of mother nature. Indo Glob J Pharm Sci. 2022;12:197–204.
3. Barua A, Junaid M, Shamsuddin T, Alam MS, Mouri NJ, Akter R, et al. Nyctanthes arbor-tristis Linn.: a review on its traditional uses, phytochemistry, pharmacological activities, and toxicity. Curr Tradit Med. 2023;9:10–22.
4. Alisherovna KM, Rustamovich TD, Baxtiyorovich UJ, Sobirovna SM. Diabetes mellitus and hyperglycemia in patients with rheumatoid arthritis. Tex J Med Sci. 2022;13:99–103.
5. Gahtori R, Tripathi AH, Chand G, Pande A, Joshi P, Rai RC, et al. Phytochemical screening of Nyctanthes arbor-tristis plant extracts and their antioxidant and antibacterial activity analysis. Appl Biochem Biotechnol. 2023;195:1–21.
6. Pamuk F, Kantarci A. Inflammation as a link between periodontal disease and obesity. Periodontol 2000. 2022;90:186–96.
7. Pundir S, Gautam GK, Zaidi S. A review on pharmacological activity of Nyctanthes arbor-tristis. Res J Pharmacogn Phytochem. 2022;14:69–72.
8. Mendie LE, Hemalatha S. Bioactive compounds from Nyctanthes arbor-tristis Linn as potential inhibitors of janus kinases (JAKs) involved in rheumatoid arthritis. Appl Biochem Biotechnol. 2023;195:314–30.
9. Saxena R, Gupta B, Saxena K, Singh R, Prasad D. Study of anti-inflammatory activity in the leaves of Nyctanthes arbor-tristis Linn—an Indian medicinal plant. J Ethnopharmacol. 1984;11:319–30.
10. Mittal I, Sarvanan K, Singh A. Formulation and evaluation of anti-osteoarthritic and anti-inflammatory activity of Nyctanthes arbor-tristis Linn as emulgel. Int J Pharm Res Appl. 2023;8:1788–98.
11. Kim MS, Kim SH. Inhibitory effect of astragalin on expression of lipopolysaccharide-induced inflammatory mediators through NF-κB in macrophages. Arch Pharm Res. 2011;34:2101–7.
12. Ahmad A, Abuzinadah MF, Alkreathy HM, Kutbi HI, Shaik NA, Ahmad V, et al. A novel polyherbal formulation containing thymoquinone attenuates carbon tetrachloride-induced hepatorenal injury in a rat model. Asian Pac J Trop Biomed. 2020;10:147–55.
13. Altemimi A, Lakhssassi N, Baharlouei A, Watson DG, Lightfoot DA. Phytochemicals: extraction, isolation, and identification of bioactive compounds from plant extracts. Plants. 2017;6:42.
14. Dinore JM, Patil HS, Dobhal BS, Farooqui M. Phytochemical analysis by GC-MS, LC-MS complementary approaches and antimicrobial activity investigation of Vigna unguiculata (L.) Walp. leaves. Nat Prod Res. 2022;36:5631–7.
15. Yatoo M, Gopalakrishnan A, Saxena A, Parray OR, Tufani NA, Chakraborty S, et al. Anti-inflammatory drugs and herbs with special emphasis on herbal medicines for countering inflammatory diseases and disorders—a review. Recent Pat Inflamm Allergy Drug Discov. 2018;12:39–58.
16. Osei Akoto C, Acheampong A, Boakye YD, Naazo AA, Adomah DH. Anti-inflammatory, antioxidant, and anthelmintic activities of Ocimum basilicum (sweet basil) fruits. J Chem. 2020;2020:2153534.
17. Gandhi Y, Kumar R, Grewal J, Rawat H, Mishra SK, Kumar V, et al. Advances in anti-inflammatory medicinal plants and phytochemicals in the management of arthritis: a comprehensive review. Food Chem Adv. 2022;1:100085.
18. Vaou N, Stavropoulou E, Voidarou C, Tsigalou C, Bezirtzoglou E. Towards advances in medicinal plant antimicrobial activity: a review study on challenges and future perspectives. Microorganisms. 2021;9:2041.
19. Zhao Y, Yang Y, Liu M, Qin X, Yu X, Zhao H, et al. COX-2 is required to mediate crosstalk of ROS-dependent activation of MAPK/NF-κB signaling with pro-inflammatory response and defense-related NO enhancement during challenge of macrophage-like cell line with Giardia duodenalis. PLoS Negl Trop Dis. 2022;16:e0010402.
20. Kim S. Exploring chemical information in PubChem. Curr Protoc. 2021;1:e217.

21. Burley SK, Bhikadiya C, Bi C, Bittrich S, Chen L, Crichlow GV, et al. RCSB protein data bank: celebrating 50 years of the PDB with new tools for understanding and visualizing biological macromolecules in 3D. Protein Sci. 2022;31:187–208.
22. Abuzinadah MF, Ahmad V, Al-Thawdi S, Zakai SA, Jamal QMS. Exploring the binding interaction of active compound of pineapple against foodborne bacteria and novel coronavirus (SARS-CoV-2) based on molecular docking and simulation studies. Nutrients. 2022;14:3045.
23. Brooks BR, Brooks CL 3rd, Mackerell AD Jr, Nilsson L, Petrella RJ, Roux B, et al. CHARMM: the biomolecular simulation program. J Comput Chem. 2009;30:1545–1614.
24. Shakya S, Khan IM, Shakya B, Siddique YH, Varshney H, Jyoti S. Protective effect of the newly synthesized and characterized charge transfer complex against arecoline induced toxicity in third-instar larvae of transgenic Drosophila melanogaster (hsp70-lacZ) Bg9: experimental and theoretical mechanistic insights. J Mater Chem B. 2023;11:1262–78.
25. Lucido MJ, Orlando BJ, Vecchio AJ, Malkowski MG. Crystal structure of aspirin-acetylated human cyclooxygenase-2: insight into the formation of products with reversed stereochemistry. Biochemistry. 2016;55:1226–38.
26. BIOVIA. Discovery Studio Visualizer. Version 21.1.0.20298. San Diego: Dassault Systèmes; 2021.
27. Bitencourt-Ferreira G, Pintro VO, de Azevedo WF. Docking with AutoDock4. In: Docking Screens for Drug Discovery. New York (NY): Humana; 2019. p. 125–48.
28. Morris GM, Goodsell DS, Halliday RS, Huey R, Hart WE, Belew RK, et al. Automated docking using a Lamarckian genetic algorithm and an empirical binding free energy function. J Comput Chem. 1998;19:1639–62.
29. Morris GM, Huey R, Olson AJ. Using AutoDock for ligand-receptor docking. Curr Protoc Bioinform. 2008;24:8–14.
30. Ravindranath PA, Forli S, Goodsell DS, Olson AJ, Sanner MF. AutoDockFR: advances in protein-ligand docking with explicitly specified binding site flexibility. PLoS Comput Biol. 2015;11:e1004586.
31. Daina A, Michielin O, Zoete V. SwissADME: a free web tool to evaluate pharmacokinetics, drug-likeness and medicinal chemistry friendliness of small molecules. Sci Rep. 2017;7:42717.
32. Jamal QMS, Khan MI, Alharbi AH, Ahmad V, Yadav BS, et al. Identification of natural compounds of the apple as inhibitors against cholinesterase for the treatment of Alzheimer's disease: an in silico molecular docking simulation and ADMET study. Nutrients. 2023;15:1579.
33. Malik MS, Faazil S, Alsharif MA, Sajid Jamal QMS, Al-Fahemi JH, Banerjee A, et al. Antibacterial properties and computational insights of potent novel linezolid-based oxazolidinones. Pharmaceuticals. 2023;16:516.
34. Pires DE, Blundell TL, Ascher DB. Platinum: a database of experimentally measured effects of mutations on structurally defined protein–ligand complexes. Nucleic Acids Res. 2015;43:D387–D391.
35. Van Der Spoel D, Lindahl E, Hess B, Groenhof G, Mark AE, Berendsen HJ. GROMACS: fast, flexible, and free. J Comput Chem. 2005;26:1701–18.
36. Zoete V, Cuendet MA, Grosdidier A, Michielin O. SwissParam: a fast force field generation tool for small organic molecules. J Comput Chem. 2011;32:2359–68.
37. Alhomrani M, Alsanie WF, Alamri AS, Alyami H, Habeeballah H, Alkhatabi HA, et al. Enhancing the antipsychotic effect of risperidone by increasing its binding affinity to serotonin receptor via picric acid: a molecular dynamics simulation. Pharmaceuticals. 2022;15:285.
38. Gupta S, Tiwari N, Verma J, Waseem M, Subbarao N, Munde M. Estimation of a stronger heparin binding locus in fibronectin domain III 14 using thermodynamics and molecular dynamics. RSC Adv. 2020;10:20288–20301.
39. Kufareva I, Abagyan R. Methods of protein structure comparison. In: Homol Model Methods Protoc. 2012;857:231–57.
40. Kuzmanic A, Zagrovic B. Determination of ensemble-average pairwise root mean-square deviation from experimental B-factors. Biophys J. 2010;98:861–71.
41. Turner P. XMGRACE, Version 5.1. Beaverton (OR): Center for Coastal and Land-Margin Research, Oregon Graduate Institute of Science and Technology; 2005.
42. Humphrey W, Dalke A, Schulten K. VMD: visual molecular dynamics. J Mol Graph. 1996;14:33–8.

43. Kumari R, Kumar R, Consortium OSDD, Lynn A. g_mmpbsa—A GROMACS tool for high-throughput MM-PBSA calculations. J Chem Inf Model. 2014;54:1951–62.
44. Baker NA, Sept D, Joseph S, Holst MJ, McCammon JA. Electrostatics of nanosystems: application to microtubules and the ribosome. Proc Natl Acad Sci USA. 2001;98:10037–41.
45. Kollman PA, Massova I, Reyes C, Kuhn B, Huo S, Chong L, et al. Calculating structures and free energies of complex molecules: combining molecular mechanics and continuum models. Acc Chem Res. 2000;33:889–97.
46. Zakiyah W, Wibowo SPS, Elyyana N, Darmawan SAN, Lestari SA, Sa'diyyah N, et al. Literature review: study of molecular mechanism level of NSAID class of drugs as COX-2 inhibitors. J EduHealth. 2022;13:572–80.
47. Muthal AP, Kulkarni R, Kumar D, Bagul C, Mukherjee-Kandhare AA, Kandhare AD, et al. Cyclic adenosine monophosphate: recent and future perspectives on various diseases. J Appl Pharm Sci. 2022;12:1–15.
48. Orhan IE, Rauf A, Saleem M, Khalil AA. Natural molecules as talented inhibitors of nucleotide pyrophosphatases/phosphodiesterases (PDEs). Curr Top Med Chem. 2022;22:209–28.
49. Paroli M, Spadea L, Caccavale R, Spadea L, Paroli MP, Nante N. The role of interleukin-17 in juvenile idiopathic arthritis: from pathogenesis to treatment. Medicina. 2022;58:1552.
50. Bi Z, Zhang W, Yan X. Anti-inflammatory and immunoregulatory effects of icariin and icaritin. Biomed Pharmacother. 2022;151:113180.
51. Arockia Babu M, Shukla R, Nath C, Kaskhedikar S. Synthesis and biological evaluation of ester derivatives of indomethacin as selective COX-2 inhibitors. Med Chem Res. 2012;21:2223–28.
52. Lin D, Xu X, Chen L, Chen L, Deng M, Chen J, et al. Supramolecular nanofiber of indomethacin derivative confers highly cyclooxygenase-2 (COX-2) selectivity and boosts anti-inflammatory efficacy. J Control Release. 2023;364:272–82.
53. Kulesza A, Paczek L, Burdzinska A. The role of COX-2 and PGE2 in the regulation of immunomodulation and other functions of mesenchymal stromal cells. Biomedicines. 2023;11:445.
54. Jogpal V, Sanduja M, Dutt R, Garg V, Tinku. Advancement of nanomedicines in chronic inflammatory disorders. Inflammopharmacology. 2022;30:355–68.
55. Rashed K. Beta-sitosterol medicinal properties: a review article. J Sci Innov Technol. 2020;9:208–12.
56. Saeidnia S, Manayi A, Gohari AR, Abdollahi M. The story of beta-sitosterol—a review. Eur J Med Plants. 2014;4:590.
57. Jin W, Dong C. IL-17 cytokines in immunity and inflammation. Emerg Microbes Infect. 2013;2:e60.
58. Tracey D, Klareskog L, Sasso EH, Salfeld JG, Tak PP. Tumor necrosis factor antagonist mechanisms of action: a comprehensive review. Pharmacol Ther. 2008;117:244–79.
59. Banner DW, D'Arcy A, Janes W, Gentz R, Schoenfeld HJ, Broger C, et al. Crystal structure of the soluble human 55 kd TNF receptor-human TNFβ complex: implications for TNF receptor activation. Cell. 1993;73:431–45.
60. Wang J, Wu Q, Ding L, Song S, Li Y, Shi L, Wang T, et al. Therapeutic effects and molecular mechanisms of bioactive compounds against respiratory diseases: traditional Chinese medicine theory and high-frequency use. Front Pharmacol. 2021;12:734450.
61. Hubbard RE, Haider MK. Hydrogen bonds in proteins: role and strength. In: Encyclopedia of Life Sciences (ELS). Chichester (UK): John Wiley & Sons, Ltd.; 2010.